

LEVEL *16*

12
B.S.

AD A088162

Semiannual Technical Summary

Graphoepitaxy

30 June 1979

Prepared for the Defense Advanced Research Projects Agency
under Electronic Systems Division Contract F19628-78-C-0002 by

Lincoln Laboratory

MASSACHUSETTS INSTITUTE OF TECHNOLOGY

LEXINGTON, MASSACHUSETTS



Approved for public release; distribution unlimited.

SDTIC
ELECTE
AUG 21 1980
D

80 8 21 042
A

DDC FILE COPY

The work reported in this document was performed at Lincoln Laboratory, a center for research operated by Massachusetts Institute of Technology. This work was sponsored by the Defense Advanced Research Projects Agency under Air Force Contract F19628-78-C-0002 (ARPA Order 3336).

This report may be reproduced to satisfy needs of U.S. Government agencies.

The views and conclusions contained in this document are those of the contractor and should not be interpreted as necessarily representing the official policies, either expressed or implied, of the United States Government.

This technical report has been reviewed and is approved for publication.

FOR THE COMMANDER

Raymond L. Loiselle

Raymond L. Loiselle, Lt. Col., USAF
Chief, ESD Lincoln Laboratory Project Office

Non-Lincoln Recipients

PLEASE DO NOT RETURN

Permission is given to destroy this document
when it is no longer needed.

MASSACHUSETTS INSTITUTE OF TECHNOLOGY
LINCOLN LABORATORY

GRAPHOEPITAXY

SEMIANNUAL TECHNICAL SUMMARY REPORT
TO THE
DEFENSE ADVANCED RESEARCH PROJECTS AGENCY

1 JANUARY - 30 JUNE 1979

ISSUED 5 JUNE 1980

Approved for public release; distribution unlimited.

A

LEXINGTON

MASSACHUSETTS

ABSTRACT

Graphoepitaxy of silicon films, 0.5 μm thick, has been achieved on amorphous fused silica substrates by laser crystallization of amorphous silicon deposited over surface-relief gratings etched into the substrates by reactive-ion etching. The gratings had a square-wave cross section with a 3.8- μm spatial period, a 100-nm depth, and corner radii of about 5 nm. The $\langle 100 \rangle$ directions in the silicon were parallel to the grating to within $\pm 15^\circ$, and perpendicular to the substrate plane to within $\pm 1.5^\circ$. A simple model for the graphoepitaxy process is presented. Sheet resistivity of phosphorus-doped graphoepitaxial silicon was 2.5 times larger than that of bulk silicon of the same doping. A technique is described for exposing patterns of spatial period p/n using near-field diffraction from masks of spatial period p . The technique, called "spatial-period-division," can be used with visible, UV or X-ray radiation. With soft X-rays, it is possible to produce gratings of much finer spatial period than can be achieved by current laser holographic methods. The feasibility of the technique was demonstrated at the 4.5-nm carbon K X-ray wavelength by "doubling" a 196.8-nm-period grating-pattern X-ray mask to produce a 98.4-nm-period pattern in polymethyl methacrylate (PMMA). Exposure of higher spatial-frequency-multiples appears feasible. A new technique for fabricating high-contrast X-ray masks with precisely controlled linewidths is described. The technique is based on the deposition at an oblique angle ("shadowing") of X-ray absorber material onto relief structures of triangular or square cross section in a polyimide plastic membrane. The triangular cross-section structures required are produced in silicon by anisotropic chemical etching and then transferred to polyimide by molding. The square cross-section structures are made by reactive-ion etching SiO_2 with CHF_3 and are transferred to polyimide by molding. Results of a numerical model of carbon K (45 \AA) X-ray exposures in PMMA of shadowed triangular profile masks are presented which indicate that linewidth control of $\pm 50 \text{\AA}$ should be possible for submicrometer period gratings. The successful replication of $< 200\text{-\AA}$ linewidth patterns in PMMA using the carbon K X-ray and shadowed square cross-section masks is reported.

CONTENTS

Abstract	iii
Introduction	v
I. Graphoepitaxy of Silicon on Fused Silica Using Surface Micropatterns and Laser Crystallization	1
II. Spatial-Period-Division - A New Technique for Exposing Submicrometer-Linewidth Periodic and Quasi-Periodic Patterns	7
III. X-Ray Lithography at $\sim 100\text{-\AA}$ Linewidths Using X-Ray Masks Fabricated by Shadowing Techniques	13
References	21

INTRODUCTION

The objectives of this research program for calendar year 1979, as stated in the proposal for renewal dated 16 October 1978, were:

- (a) Determine if surface-relief structures in SiO_2 or Si_3N_4 can induce oriented single-crystal growth of silicon and/or gallium arsenide.
- (b) Conduct basic studies, by transmission microscopy (TEM), of thin-film nucleation and growth on surface-relief structures.
- (c) Conduct studies of laser annealing of silicon and gallium arsenide over surface-relief structures in SiO_2 and Si_3N_4 .
- (d) Improve technology of surface-relief-structure fabrication to provide finer spatial periods, sharper corners, smoother sidewalls, and straighter edges.

Objective (a) was achieved in the fourth quarter of 1978: uniformly oriented crystalline films of silicon were produced by laser crystallization of amorphous silicon over surface-relief gratings in amorphous SiO_2 . As a result of this success, the objectives for calendar year 1979 were as follows:

- (a) Improve the crystallographic and electrical properties and the surface smoothness of silicon produced by graphoepitaxy.*
- (b) Conduct basic studies, by TEM, of thin-film nucleation and growth on surface-relief structures [same as (b) above].
- (c) Develop means of achieving graphoepitaxy of Si and GaAs that do not involve laser crystallization.
- (d) Improve technology of surface-relief-structure fabrication to provide finer spatial periods, sharper corners, smoother sidewalls, and straighter edges [same as (d) above].
- (e) Fabricate simple diodes and transistors in silicon and/or GaAs oriented by graphoepitaxy.*

This report describes progress on items (a) and (d)

* A new term we coined for the process of orienting overlayer films by means of surface-relief patterns.

GRAPHOEPI TAXY

I. GRAPHOEPI TAXY OF SILICON ON FUSED SILICA USING SURFACE MICROPATTERNS AND LASER CRYSTALLIZATION

In earlier papers,¹⁻⁵ we proposed the use of artificial microstructures, fabricated on a substrate surface, to manipulate the nucleation, growth, and orientation of overlayers, and demonstrated uniform orientation of KCl (Refs. 2 and 3), nematic and smectic A liquid crystals^{2,4} and, more recently, silicon.⁶ We proposed that the term "graphoepitaxy" be used to cover any form of orientation induced by artificial surface patterns.⁶ In this report, we present a simple model for graphoepitaxy of solid crystalline films on amorphous substrates, give additional details on silicon graphoepitaxy, including electrical characterization, and discuss some future implications for microelectronic devices and solar cells.

A theoretical model of the graphoepitaxy process² predicts that film formation methods that yield textured polycrystalline films (i.e., the individual crystal grains have one particular plane parallel to the substrate surface and random orientation otherwise) on smooth amorphous substrates should yield uniformly oriented films if such film formation is carried out over an appropriate surface-relief structure in the amorphous substrate. For example, if a film formation method yields a (100) texture (i.e., {100} planes of grains are parallel to the substrate surface but orientation is random in the surface plane) on a smooth amorphous substrate, such as depicted in Fig. 1(a), then the same method should yield a uniformly oriented film on the structures depicted in Figs. 1(b) and (c), provided the spatial period of the grating is small compared with the normal grain size. Polycrystalline films that exhibit (111) texture on a smooth amorphous substrate would require relief structures such as depicted in Figs. 2(b), (c), and (d), in order to be oriented uniformly. An important conclusion from the theoretical model is that film formation methods that closely approach equilibrium are preferred for graphoepitaxy.

With current technology it is easier to fabricate square-wave cross sections⁷ than the other cross sections depicted in Figs. 1 and 2 [the triangular cross sections are easily fabricated in single-crystal substrates⁸ but not directly in amorphous material; a structure approaching that in Fig. 2(d) can be fabricated in carbonaceous substrates⁹] and thus, in order to achieve uniform orientation of silicon on an amorphous substrate, we sought film formation methods that yielded (100) or (110) texture. We found that under certain conditions laser crystallization of amorphous silicon over fused silica yields a polycrystalline film having a nearly perfect (100) texture, with grains several tens of micrometers in diameter.⁶ The full details of the initial silicon graphoepitaxy experiments are given elsewhere.⁶ The essential details are as follows: the relief grating, of 3.8- μm spatial period, was etched into fused silica substrates to a depth of 100 nm by reactive-ion etching, using a grating of thin-film chromium as the mask. Sidewalls were within 6° of vertical, and the radii of curvature at the corners where the sidewalls join the tops and groove bottoms were about 5 nm. For crystallographic orientation experiments, about 0.5 μm of amorphous silicon was deposited by a CVD process over the relief grating as illustrated in Fig. 3(a). The silicon was laser crystallized, both inside and outside the grating area, using an argon laser and an apparatus that scanned the substrate past the laser beam in a raster fashion, as depicted in Fig. 4. The laser delivered 6 W into a spot about 400 μm in diameter.

The initial raster scan produced polycrystalline silicon having grains 10 to 20 μm in diameter, with (100) texture. With additional raster scans, the grains grew to about 100- μm diameter

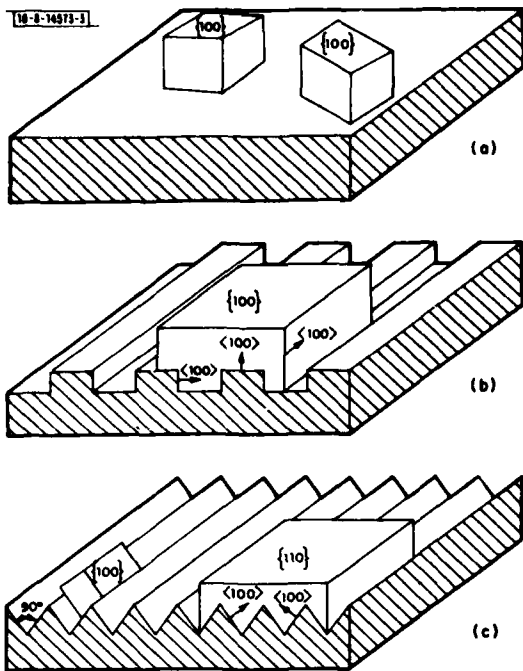


Fig. 1. Schematic illustration of (a) grains of a polycrystalline film that exhibits (100) texture on a smooth amorphous substrate (i.e., {100} planes are parallel to the substrate surface but orientation is random otherwise); (b) uniform (100) orientation obtained when the (100) textured film is formed on a square-wave relief structure; (c) uniform (110) orientation obtained when the (100) textured film is formed on a 90° "sawtooth" structure.

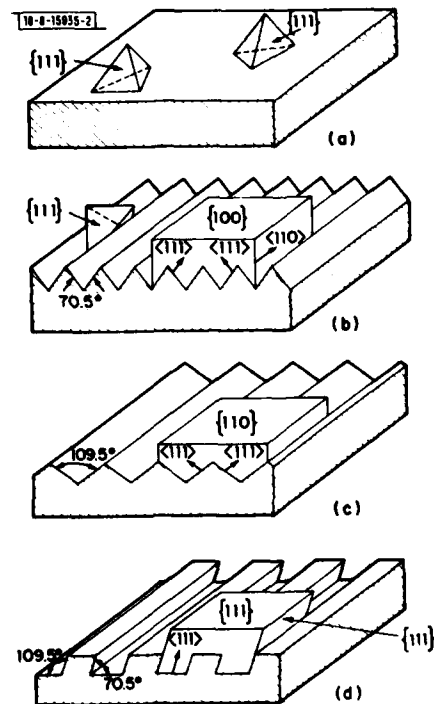


Fig. 2. Schematic illustration of (a) grains of a polycrystalline film that exhibits a (111) texture on a smooth amorphous substrate (i.e., {111} planes are parallel to the substrate surface but orientation is random otherwise); (b) uniform (100) orientation obtained when the (111) textured film is formed on a 70.5° "sawtooth" structure; (c) uniform (110) orientation obtained when the (111) textured film is formed on a 109.5° "sawtooth" structure; (d) uniform (111) orientation obtained when the (111) textured film is formed on a relief grating with facets intersecting at 109.5° and 70.5°.

Fig. 3. Schematic illustration of (a) an amorphous silicon film, 0.5 μm thick, deposited by a CVD process over a surface-relief grating in fused silica; (b) a uniformly oriented film of silicon obtained by laser crystallization of the amorphous silicon over the relief structure. The crystallographic axes indicate the mean orientation of the crystallized silicon. Note that in (b) the top surface of the silicon does not follow the contour of the grating, as in (a). In practice, the surface of the silicon in (b) has a roughness of several tens of nanometers.

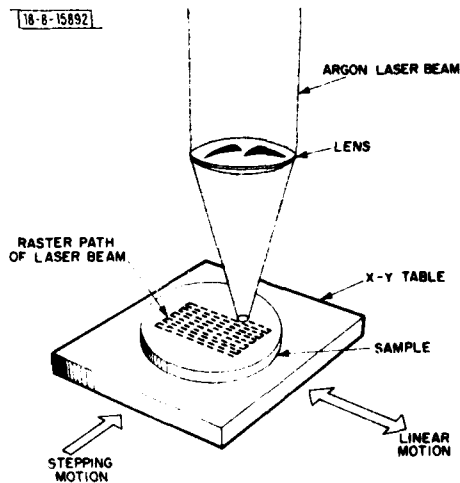
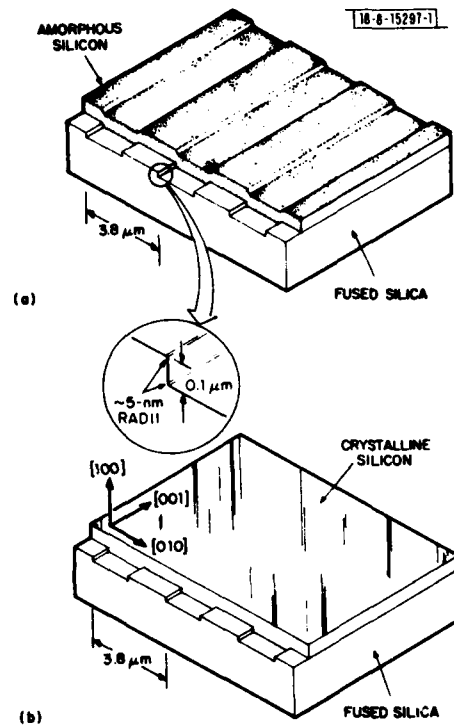


Fig. 4. Schematic illustration of the scanning apparatus used for the laser crystallization. The laser was operated multi-line with power level between 6 and 7 W. The lens had a focal length of 60 mm and was placed 45 mm or less in front of the substrate. Typically, a scanning speed of 10 mm/sec was used, and successive horizontal scans were separated by 12 μm .

and the silicon became progressively better oriented relative to the grating. The initial experiments used reflection electron diffraction (RED) to analyze the orientation and texture. This method, which samples only the material within ~ 10 nm of the top surface, indicated that after four raster scans a highly preferred orientation relative to the grating was obtained where the mean [100] directions in the silicon are parallel to grating and perpendicular to the substrate surface, as illustrated schematically in Fig. 3(b). Orientation was found to be independent of laser scan direction, but strongly dependent on the sharpness of the cross-sectional profile of the relief grating.

Since publication of our initial results, we have set up an X-ray pole plotting apparatus which permits a more quantitative evaluation of orientation and texture than RED. Measurements of the width of the (400) diffraction peak, as a function of angle relative to the substrate normal, and the widths of the four (220) peaks, as a function of rotation about the substrate normal, indicated that there was a distribution of orientation in the graphoepitaxial silicon prepared as described above. On $3.8\text{-}\mu\text{m}$ spatial-period surface gratings, the [100] directions are parallel to the grating to within $\pm 15^\circ$ and perpendicular to the substrate surface to within $\pm 1.5^\circ$. Decreasing the grating spatial period, increasing the grating depth, improving the cross-sectional profile and line-edge smoothness, increasing the substrate temperature during crystallization, and increasing the number of raster scans all serve to decrease the spread in orientations. At present, the influences of these parameters are being systematically investigated. We are confident that with further development films prepared by graphoepitaxy will more closely approach the ideal of the "single crystal."

The silicon was separated from the fused silica substrate by immersion in concentrated HF and viewed in a transmission electron microscope (TEM). Distinct grains were clearly discernible in the silicon from outside the grating area, but no grain boundaries were visible in the silicon from inside the grating area although the X-ray results indicate the presence of distinct grains. No slip planes, dislocation loops or twins were observed by TEM. Figure 5 shows a

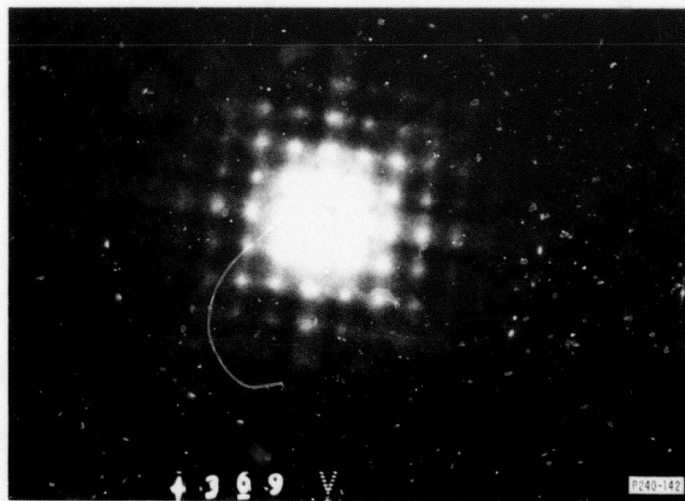


Fig. 5. Transmission electron diffraction pattern of a 500-nm-thick silicon film laser crystallized over a $3.8\text{-}\mu\text{m}$ -period square-wave grating in amorphous fused silica. The electron beam was perpendicular to the silicon film yielding a (100) diffraction pattern. The Kikuchi lines visible in the pattern indicate a high degree of crystalline perfection.

transmission diffraction pattern taken in the TEM of the silicon over the grating. The Kikuchi lines in the diffraction pattern indicate a highly ordered crystalline structure.

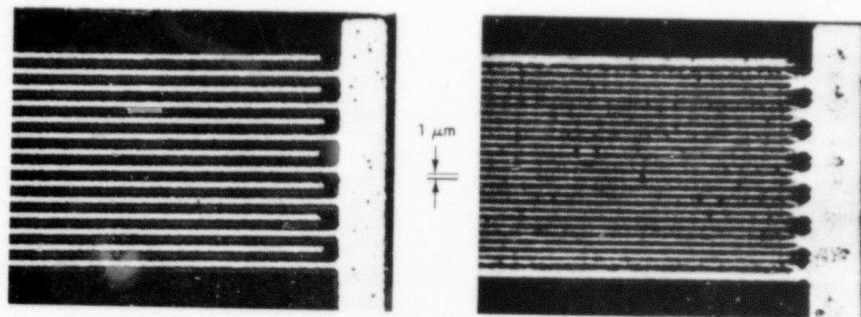
The graphoepitaxial silicon films have an irregular surface roughness with amplitude of several 10 nm and minimum period typically $\gtrsim 50 \mu\text{m}$. In addition, there are intersecting microcracks, with separation ranging from tens of micrometers to $\sim 1 \text{ mm}$. These microcracks tend to lie along major crystallographic directions, particularly $\langle 110 \rangle$. We believe these cracks are due to stresses induced by laser crystallization. Fewer microcracks form if the substrate is heated to a few hundred degrees centigrade during laser crystallization. Because of surface roughness and microcracks, we did not attempt to fabricate devices or make Hall mobility measurements on this material. We have however, made Schottky diodes and measured sheet resistivity.

Amorphous silicon films $0.5 \mu\text{m}$ thick on top of surface gratings were doped by ion implantation with boron or phosphorus prior to laser crystallization, using four different ion energies so as to achieve a nearly uniform doping of 2.4×10^{17} atoms/cm³ throughout the silicon film. Subsequent laser crystallization both activated the dopant and induced uniform orientation. Bulk silicon wafers were also implanted in the same manner to serve as controls. The phosphorus was implanted in 35- Ω -cm p-type wafers and the boron was implanted in 30- Ω -cm n-type wafers. These silicon wafers were then annealed at 900°C for 30 min. Four in-line Cr/Au dots (1.4 mm in diameter, spaced 1.5 mm apart) were fabricated on the surfaces of both the graphoepitaxial silicon and the control wafers, enabling "four point probe" measurements to be made. The samples of graphoepitaxial silicon showed a large variation in sheet resistance depending upon the substrate temperature during laser crystallization. The best results were obtained on phosphorus-implanted samples which were mounted on a heating stage held at 540°C during laser crystallization. The sheet resistance was a factor of 2.5 times larger than that of the phosphorus-doped silicon wafer used as a control. Thus, the mobility of electrons in the graphoepitaxial silicon is at least 40 percent of bulk mobility, and very likely better than this since surface roughness and microcracks in the 0.5- μm -thick silicon almost certainly produce scattering and reduce the apparent mobility.

Silicon on an insulating substrate is a very attractive medium for integrated electronic devices, particularly at submicrometer linewidths. Promising results have been obtained with large-grain polycrystalline silicon¹⁰ and small islands of single-crystal silicon¹¹ on Si_3N_4 and SiO_2 . Silicon-on-sapphire (SOS), which is available commercially, suffers from a number of problems, including aluminum auto-doping and crystalline defects. Graphoepitaxy of silicon offers many more degrees of freedom in the choice of substrate, film orientation, and growth parameters than the SOS process. Although the material is not yet suitable for fabrication of high quality devices, results are very promising after less than two man-years spent directly on silicon graphoepitaxy. The problems of microcracks and surface roughness described above may be circumvented by replacing the laser crystallization with a process of direct growth on relief structures. Alternatively, if the amorphous silicon is formed into separate islands^{2,11} prior to laser crystallization, the microcracks can be avoided.

Graphoepitaxy of silicon also offers the possibility of forming single-crystal films, and hence electronic devices, over amorphous layers on top of other devices. This capability could lead to three-dimensional integration and radically new configurations. Graphoepitaxy also may provide new and energy conserving means of making solar cells.

We have recently learned of work by N. N. Sheftal and colleagues in the Soviet Union in which artificial surface structures were used in crystal growth studies.¹² The objectives of these



P240-157

Fig. 6. The left half is an optical micrograph of an interdigital pattern that had been RF sputter etched into chromium on a photomask. The spatial period of the grating is $2.54 \mu\text{m}$. When exposed in photoresist at a mask-to-resist gap of about $8 \mu\text{m}$, the second spatial-frequency-multiple ($1.27\text{-}\mu\text{m}$ period) was imaged in the resist. Subsequent RF sputter etching yielded the pattern in chromium shown in the right half.

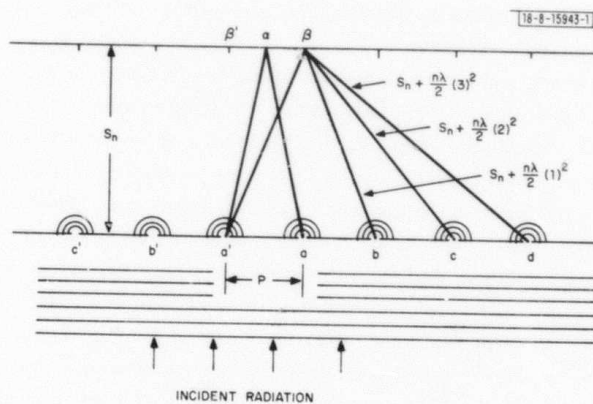


Fig. 7. A simple model, reminiscent of explanations in elementary physics texts of Young's famous double slit experiment of 1801, of spatial-period-division.

studies appeared to be to demonstrate that microcrystals (1 to 10 μm in size) form in a medium and can align and attach themselves to a growth surface.

M. W. Geis H. I. Smith
D. C. Flanders D. A. Antoniadis

II. SPATIAL-PERIOD-DIVISION - A NEW TECHNIQUE FOR EXPOSING SUBMICROMETER-LINEWIDTH PERIODIC AND QUASI-PERIODIC PATTERNS

Periodic and quasi-periodic structures of submicrometer spatial period are of fundamental importance in a number of areas: guided wave optics,¹³ distributive-feedback and distributed-Bragg-reflector lasers,¹⁴ graphoepitaxy,^{3,6} and planar superlattice electronic devices.¹⁵ In addition, high-quality periodic structures are essential elements in optics and spectroscopy at all wavelengths, and serve as calibration standards for scanning electron beam systems.^{16,17} For spatial periods from about 2 to $\sim 0.2 \mu\text{m}$, holographic lithography has been the preferred method of exposing periodic and quasi-periodic patterns, either directly on substrates of interest or on masks which are subsequently replicated photolithographically or with soft X-rays.¹⁸ Holography in high-refractive-index media has been used to expose gratings of 110-nm period,¹⁹ but the technique used is cumbersome, and cannot be extended much below about 70 nm. Sources with wavelengths shorter than the He: Cd laser (325 nm) generally have limited coherence length and poor mode quality, or require complex apparatus for up-conversion.²⁰ Here we report a conceptually simple technique for exposing periodic and quasi-periodic structures which should be especially attractive for exposing spatial periods below 100 nm. Gratings with spatial periods below 100 nm will be important in the application cited above and also in very-far UV and X-ray optics, fields which are likely to grow considerably in the near future. The technique, which we call spatial-period-division, employs near-field diffraction from periodic and quasi-periodic "parent" masks to produce intensity patterns with spatial periods finer than the parent mask. This phenomenon was observed long ago with visible light and has been studied by several researchers.²¹ What is new in our work is its use in microlithography, especially in conjunction with soft X-ray lithography.

In this Laboratory, spatial-period-division was first observed in 1968 during studies of photolithographic shadow printing and the influence of mask-to-substrate gap. Figure 6 illustrates the "doubling" of a grating of spatial period 2.54 μm by shadow printing it at a gap of about 8 μm , yielding a grating of 1.27- μm spatial period. In this report, we describe the technique of spatial-period-division and demonstrate the "doubling" of a 196.8-nm spatial-period grating by X-ray shadow printing at a gap of 4.3 μm , yielding a grating of 98.4 nm.

The theory of spatial-period-division will be discussed in detail elsewhere. For the present, the simple model depicted in Fig. 7 is sufficient to illustrate the basic principles. A periodic array of slits is illuminated with radiation from a distant point source. Radiation from slits a and a' will be in phase, and produce an intensity maximum at point α for all distances S . However, at a certain distance, S_2 , the difference in length between paths $a'\beta$ and $a\beta$ will be one wavelength, and the path lengths from slits b, c, d , etc., to β will differ from $a\beta$ by integral multiples of λ . The result is an intensity maximum at β and, by symmetry, also at β' . This intensity pattern, with maxima at β', α , and β , will have spatial period $p/2$ and thus corresponds to a "doubling" of the original grating's spatial frequency. The model is easily generalized to predict other spatial-frequency-multiples [i.e., tripling ($n = 3$), quadrupling ($n = 4$), etc.] at distances given by

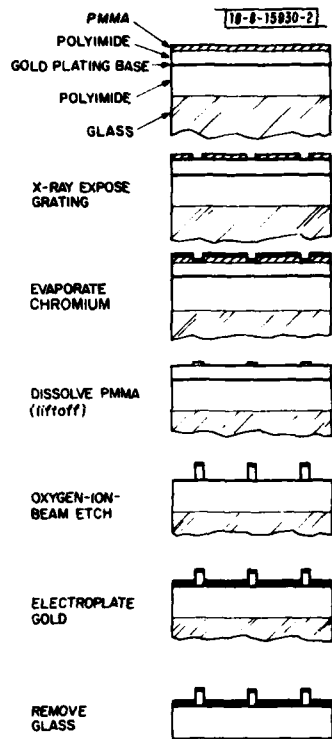


Fig. 8. Procedure for fabricating the parent X-ray mask having slit openings equal to $1/4$ of the grating period, p . A film of PMMA is exposed using an X-ray mask having slits of width $p/4$. About 20 nm of chromium is evaporated and a grating pattern with lines of $p/4$ width is produced by liftoff. Slots are etched in the polyimide down to a gold plating base using an oxygen ion beam (Ref.9). Gold is electroplated to at least 200-nm thickness. Finally, the glass substrate is etched in hydrofluoric acid.

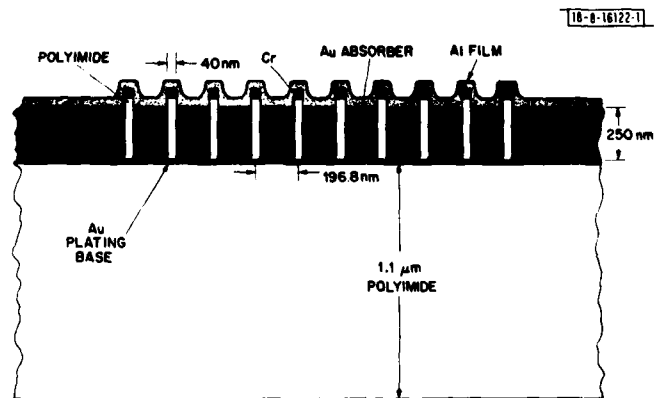


Fig. 9. Cross-sectional diagram of the 196.8-nm-period parent mask used in the present experiments to expose the second spatial-frequency-multiple: a 98.4-nm-period grating. In reality, the mask was not the idealized structure depicted, but instead the gold electroplating exceeded the height of the polyimide and bridged across. This led to underexposure of the final "doubled" pattern.

$$S_n = p^2/n\lambda$$

where n is an integer greater than one. The intensity patterns of the spatial-frequency-multiples depend critically on the width of the slits in the parent mask. For monochromatic collimated radiation, the 3-dB width of the intensity peaks is approximately equal to the width of the slits. If the source has some angular divergence and a moderate bandwidth (~20 percent), the intensity patterns of the spatial-frequency-multiples will be approximately sinusoidal, superimposed on a low-level background. Such patterns will be adequate for exposure of high-contrast resists such as PMMA over depths of field, ΔS_n , given approximately by

$$\begin{aligned} \Delta S_n &\sim \frac{1}{2} \left(\frac{S_{n-1} - S_{n+1}}{2} \right) \\ &\sim \frac{p^2}{2\lambda(n^2 - 1)} \end{aligned}$$

Theory predicts that the quality of the n^{th} spatial-frequency-multiple will be optimized (i.e., spatial-harmonics less than n are minimized) if the slit width is $\leq p/2n$. Thus, for "doubling," the slits of the parent mask should have widths $\leq p/4$.

Experiments

For experimental verification of spatial-period-division using soft X-rays, a synchrotron would be an ideal source. Since one was not readily available to us, we used a simple laboratory source of carbon K soft X-rays ($\lambda = 4.5$ nm), and also did light-optical ($\lambda \sim 600$ nm) simulation of the X-ray exposure. The X-ray parent mask had a grating pattern of 196.8-nm spatial period with slits 40 nm wide, approximately the optimum slit-width for doubling. An oblique-shadowing technique²² was used to produce a first mask having absorber stripes effectively 40 nm wide. This first mask was then "reversed in polarity" onto a second mask, using a lift-off process, to yield a mask with 40-nm-wide opening in gold 40 nm thick. The procedure outlined in Fig. 8 was then used to obtain 40-nm-wide slits in 250-nm-thick gold. Figure 9 depicts the cross section of the finished parent mask. In order to expose a pattern with twice the spatial frequency of the parent mask (i.e., doubling), a gap, S_2 , of 4.3 μm is required between the parent mask's grating and the resist film. Figure 10 illustrates the assembly we used to establish and control this gap. The solid portions of the spacer membrane attenuate the carbon K X-rays by 9 dB and thus the image is underexposed here.

Penumbra, due to the finite size of our source, determined how close the mask-substrate assembly could be brought to the X-ray source, and thus determined exposure time. The penumbra is given by

$$\delta = S d/D$$

where D is the source-to-mask distance, S is the mask-to-substrate gap, and d is the source diameter. For doubling a 196.8-nm period grating, $S = 4.3$ μm , and δ must be < 196.8 nm/4. Our source diameter is 1 mm, and thus D must be > 87 mm. We used a D of 115 mm, which corresponds to an exposure time of 21 hr for the carbon K source operated at 4.8 kV and 70 mA. For comparison, Table I lists exposure times for a variety of spatial-frequency-multiples and two parent mask periods, assuming a synchrotron source. In the absence of a synchrotron or

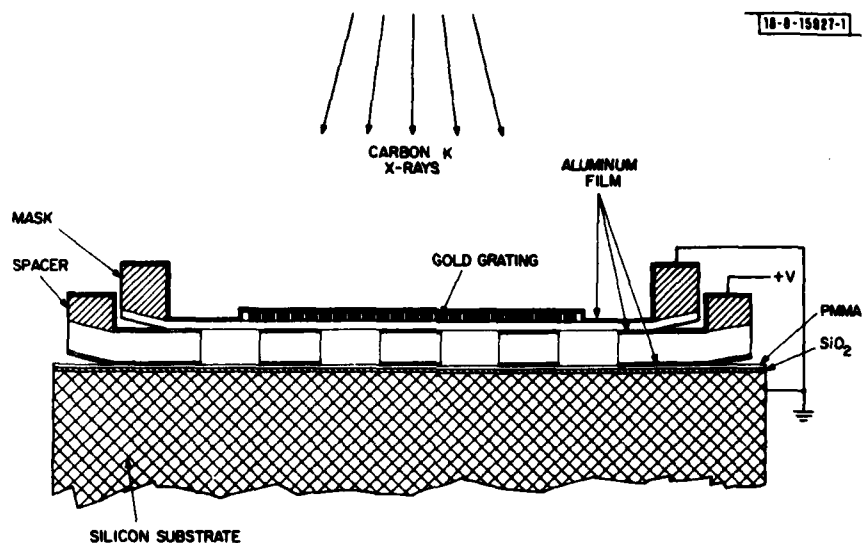


Fig. 10. Assembly used to maintain a well-defined spacing between parent mask and substrate resist film during exposure. The spacer is a polyimide membrane having rectangular holes $25 \times 25 \mu\text{m}$. It is coated on both sides with an aluminum film so that a voltage applied, as illustrated, will hold the mask-spacer-substrate assembly together as shown.

	Multiple	GAP (μm)	Approximate Depth of Field (μm)	Period Produced (μm)	Exposure* Time (sec)
1.0- μm -Period Parent Mask (10-nm slits)	2nd	98.0	32.7	0.5	2
	3rd	65.4	12.2	0.33	3
	4th	49.0	6.5	0.25	4
	5th	39.2	4.1	0.20	5
0.2- μm -Period Parent Mask (10-nm slits)	2nd	3.92	1.3	0.1	2
	3rd	2.61	0.5	0.067	3
	4th	1.96	0.26	0.05	4
	5th	1.57	0.16	0.04	5

* Calculated exposure times for PMMA and a source intensity of 1 W/cm^2 .

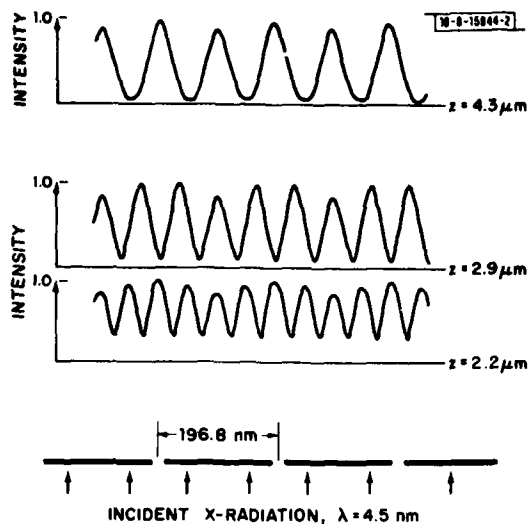


Fig. 11. Numerical calculations of the intensity of the second, third, and fourth spatial-frequency-multiples of a 196.8-nm-period parent mask, assuming the cross-sectional profile as shown in Fig. 9, an X-ray source of 1-mm diameter and a source-to-mask distance of 115 mm.

storage ring, one might reduce exposure times by using a source of smaller diameter or linear geometry. Hot plasma sources²³ may be attractive for this application.

Figure 11 shows intensity plots for the second, third, and fourth spatial-frequency-multiples of the 196.8-nm period grating. The plots were calculated numerically, taking into account the angular divergence of the X-rays from our source. To test these predictions, we set up a light-optical simulation of our X-ray configuration. The scale factor was approximately 100, that is, in place of the 4.5-nm X-rays, we used white light with an orange filter, and in place of the 196.8-nm-period grating X-ray mask, we used a photomask having a 16.9- μm -period grating etched in chromium. The chromium mask was exposed by electron beam lithography and had slit widths of 1.7 μm . Figure 12 shows the results of the optical simulation, as recorded on photographic film.

Figure 13 demonstrates doubling of the 196.8-nm-period X-ray mask. The mask was not the ideal structure depicted in Fig. 9. Gold had overplated the slots in the polyimide and bridged across. Further development of the spatial-period-division technique is called for and should be a welcome challenge for those seeking to push periodic and quasi-periodic structures into the domain below 100 nm. In principle, the technique can be extended down to the limit of microlithography, which is believed to be about 10-nm spatial period.

Spatial-period-division as described above requires a high attenuation (>20 dB) of the incident radiation through the absorbing regions of the parent mask. Otherwise, the radiation transmitted through the absorber can interfere with the diffracted radiation (the simple model in Fig. 7 assumes transmission only through the slits) producing undesirable spatial-harmonic components. Alternatively, if 50 percent of the incident radiation is phase shifted by π in passing through the mask pattern, the zero-order diffracted beam can be canceled.²⁴ If $p < 2\lambda$, only the first-order diffracted beams will be present, and their interference will produce only

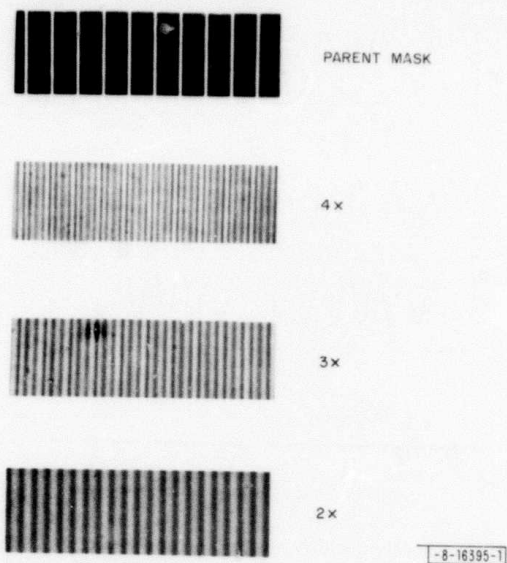


Fig. 12. Results of an optical simulation of the experiment to X-ray expose the second spatial-frequency-multiple of the 196.8-nm-period X-ray mask. The optical simulation was at a scale-up of about 100 (i.e., 0.6- μm wavelength vs 4.5-nm X-ray wavelength). The second, third, and fourth spatial-frequency-multiples of a 16.9- μm spatial-period photomask, as exposed in photographic film, are shown. The light source was an incandescent lamp with an orange filter.

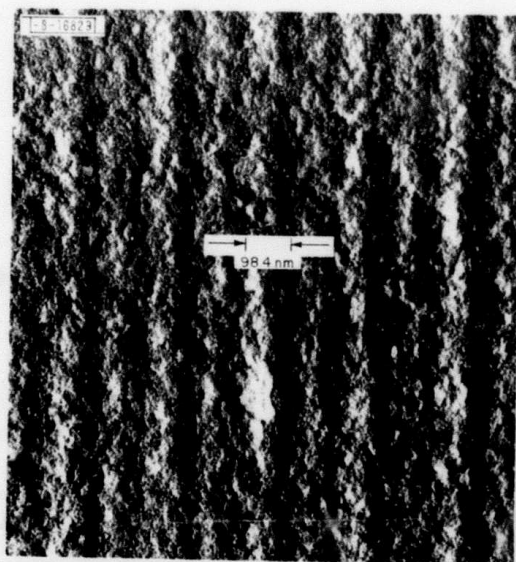


Fig. 13. Exposure in PMMA (average molecular weight = 950,000) of a 98.4-nm spatial-period grating by means of spatial-period-division. The 98.4-nm-period pattern is the second spatial-frequency-multiple of the 196.8-nm-period X-ray mask, depicted in Fig. 9.

the second spatial-frequency-multiple. At optical and UV wavelengths it is easy to achieve both zero-order cancellation and $p < 2\lambda$. At 4.5-nm wavelength, on the other hand, gold attenuates 128 dB/ μm , and the phase shift is approximately $1^\circ/\text{nm}$. Both high attenuation (>20 dB) and a π phase shift require a thick absorber (~ 200 nm). This is possible using electroplating as illustrated in Figs. 8 and 9.

If the parent mask introduces a phase shift of π thereby canceling the zero-order beam, and if $p < 2\lambda$, doubling of any spatial frequency occurs at all distances. Thus, one could double quasi-periodic structures such as variable period gratings, grids, and Fresnel zone plates. This might be especially important in making structures for X-ray imaging.

Spatial-period-division provides a simple means of exposing large-area, low-distortion, periodic structures. It has several advantages over conventional holographic lithography: spatial periods below 100 nm are readily exposed; when used with soft X-rays reflection from substrates is avoided thereby permitting high aspect-ratio resist structures; the profile of the intensity pattern can be altered by varying the parent-mask slit width.

D. C. Flanders
A. M. Hawryluk
H. I. Smith

III. X-RAY LITHOGRAPHY AT $\sim 100\text{-}\text{\AA}$ LINEWIDTHS USING X-RAY MASKS FABRICATED BY SHADOWING TECHNIQUES

Submicrometer spatial-period grating patterns have found wide application in several fields. Some recent examples include optical and X-ray diffraction gratings,^{25,26} integrated optical devices,¹⁴ liquid crystal displays,²⁷ and oriented crystal growth on amorphous substrates.³ In most cases, submicrometer spatial-period grating patterns were generated using holographic lithography, although some work has been done using scanning electron beam lithography (SEBL). Holographic lithography can yield large area gratings with very accurate periodicity and low distortion. However, the ratio of linewidth to grating period is difficult to control and the rounded resist profiles, which are characteristic of holographic lithography, often limit subsequent processing. Gratings generated by SEBL do not generally have the same freedom from distortion over large areas that is characteristic of holographic gratings. Under certain conditions nearly vertical walled resist profiles can be obtained with SEBL; however, precise control of the ratio of linewidth to period of submicrometer period gratings is difficult because of limited contrast in the exposure caused by electron backscattering. Writing times also tend to be very long for large area gratings. X-ray lithography using PMMA resist and the carbon K (45 \AA) X-ray is capable of producing vertical walled resist profiles²⁰ in thick PMMA and is believed to be capable of 50- \AA resolution.^{28,29} Thus the problem of exposing grating patterns of precisely controlled linewidths comes down to one of making an X-ray mask with sufficient contrast and the proper linewidths.

In this report, a new technique for fabricating high-contrast X-ray masks with precisely controlled linewidths as small as 100 \AA is described. The technique is based on the deposition at an oblique angle ("shadowing") of X-ray absorber material onto relief structures of triangular and square cross section in a polyimide membrane. The success of the technique depends on the perfection of the relief structures. Extremely smooth and reproducible triangular cross-section surface-relief structures can be fabricated in single-crystal silicon by anisotropic chemical etching,⁸ and square cross-section surface-relief structures with smooth vertical sidewalls and sharp corners can be fabricated in silicon dioxide by reactive-ion etching in

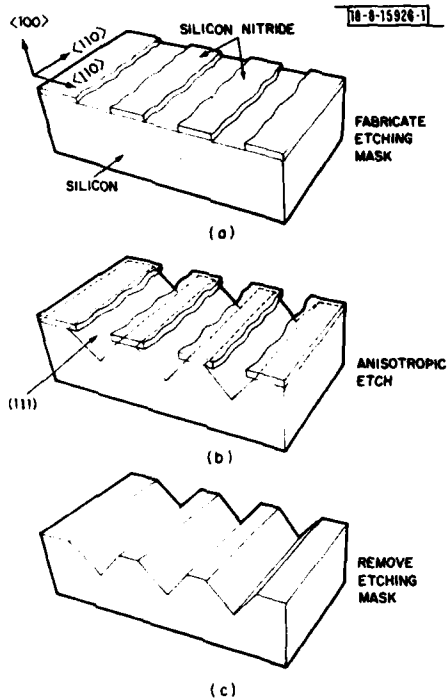


Fig. 14. Sequence of steps to fabricate a precisely defined triangular profile surface-relief structure in single-crystal silicon by anisotropic etching.

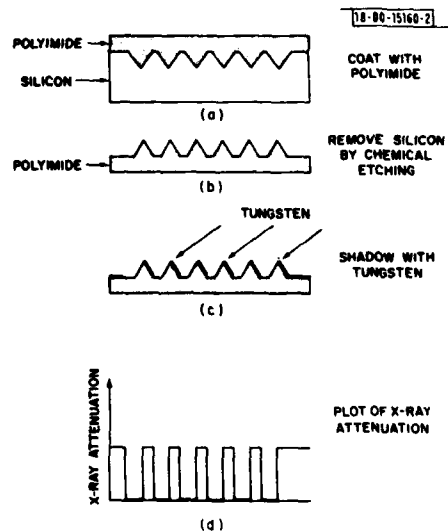


Fig. 15. Fabrication procedure for shadowed triangular profile polyimide membrane X-ray mask and the resulting carbon K X-ray attenuation. The X-ray mask linewidth can be varied by varying the shadowing angle.

CHF_3 gas (Ref. 20). These structures can then be transferred to a thin polyimide plastic membrane by molding. In the case of the triangular cross section, the linewidth of the final pattern is precisely determined by the shadowing angle. For the square cross section, the thickness of the absorber material on the vertical sidewall determines the linewidth.

The procedure for fabricating triangular surface-relief structures in silicon is shown in Fig. 14. A (100)-oriented silicon wafer is coated with $\sim 200 \text{ \AA}$ of Si_3N_4 by chemical vapor deposition and a 50-\AA -thick layer of chromium is evaporated onto the Si_3N_4 . A grating pattern with the grating lines parallel to the $\langle 110 \rangle$ direction in the silicon is exposed in $\sim 750 \text{ \AA}$ of Shipley AZ-1350B photoresist using holographic lithography. The chromium is then chemically etched,³⁰ the Si_3N_4 is reactive-ion etched in a CHF_3 plasma using the chromium as a mask, and finally the chromium is chemically removed. The resulting structure is depicted in Fig. 14(a). Although the period of the grating is precisely controlled by the configuration of the holographic lithography system, the Si_3N_4 grating linewidth can vary considerably over the sample and the line edges can be quite rough. The sample is immersed in a potassium hydroxide solution which etches in the $\langle 111 \rangle$ direction in the silicon much more slowly than all other directions.⁸ Very smooth (111) plane facets, whose angle of intersection (70.5°) is precisely determined by the crystal structure, rapidly form and the etching essentially ceases once the structure shown in Fig. 14(b) is achieved. The Si_3N_4 is removed in concentrated hydrofluoric acid. The relief structure in the silicon surface is covered with a liquid polyimide plastic³¹ as shown in Fig. 15(a). The plastic is polymerized by heating and removed from the silicon mold by peeling after very brief immersion in diluted HF or by etching away the substrate in 96% HF, 4% HNO_3 . The polyimide membrane surface-relief structure is mounted on a metal or plastic ring and shadowed with an X-ray absorber material as shown in Fig. 15(c). Tungsten was chosen as the absorber material because it has a large X-ray absorption of $158 \text{ dB}/\mu\text{m}$ at the carbon K X-ray³² and has a small grain size. Obviously, the linewidth of the projection of the X-ray absorber pattern can be varied by choosing the shadowing angle.

Figure 16(a) shows the mask structure which is obtained when a 3200-\AA -period triangular profile polyimide grating is shadowed with 200 \AA of tungsten at 14.5° . The attenuation of

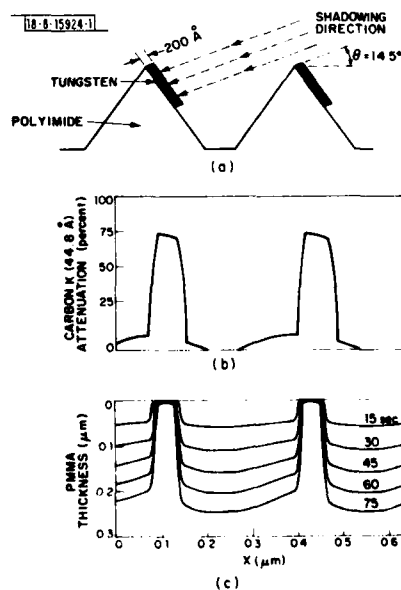


Fig. 16. (a) Schematic representation of a 3200-\AA -period triangular profile X-ray mask shadowed at 14.5° with 200 \AA of tungsten; (b) carbon K X-ray attenuation at normal incidence for the mask structure shown in (a); (c) calculated PMMA profile for several development times for a simulated carbon K X-ray exposure using the mask illustrated in (a).

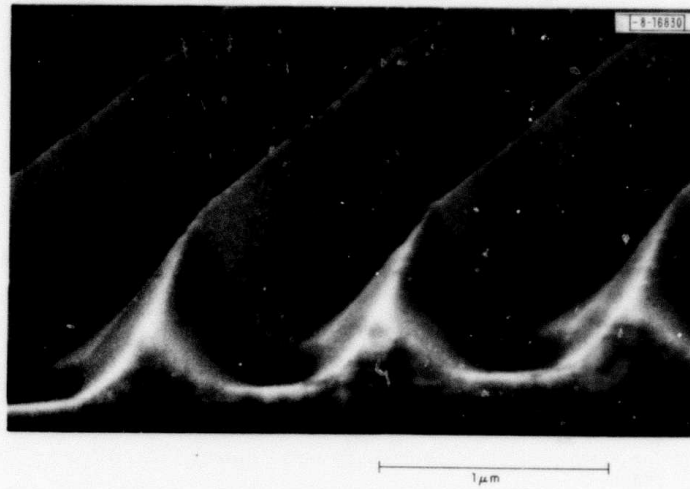


Fig. 17. SEM micrograph of a 1- μm -period relief structure fabricated in polyimide by the process depicted in Figs. 14 and 15.

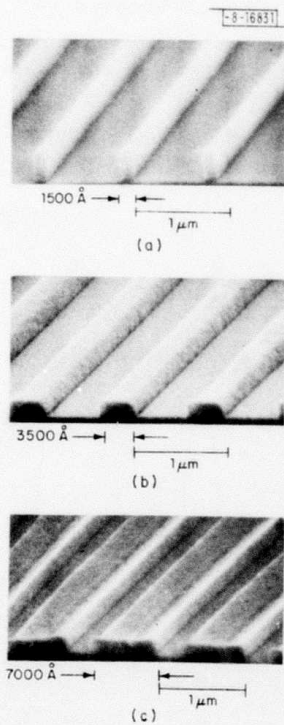


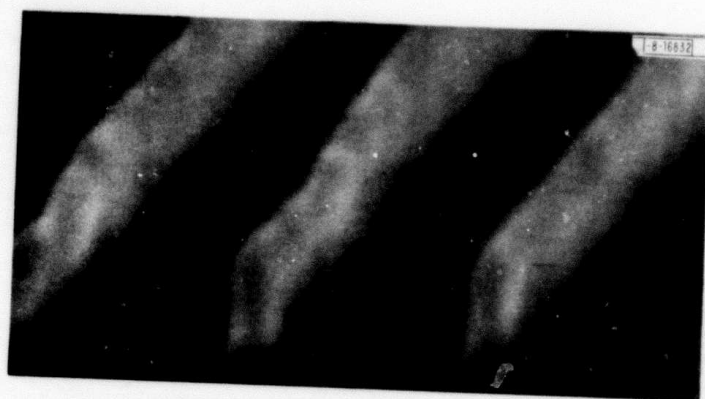
Fig. 18. SEM micrographs of 1- μm -period PMMA gratings on amorphous SiO_2 substrates produced by carbon K X-ray lithographic replication of 1- μm -period triangular profile polyimide masks shadowed with 200 \AA of tungsten at (a) 19° , (b) 33° , and (c) both sides at 33° .

carbon K X-rays passing through the mask at normal incidence is plotted in Fig. 16(b). A simulation of the cross-sectional profile that would be developed in a PMMA resist film based on the data in Fig. 16(b) is shown in Fig. 16(c). Results for several development times are shown. Note the sharp vertical sidewalls and small change in linewidth with development time. The PMMA profile is calculated numerically by assuming that development is a simple surface-etching process in which the etching rate at any point is proportional to the 3.4 power of the energy absorbed in the PMMA at that point;³³ diffraction is neglected. This development model is believed to be qualitatively correct for PMMA for carbon K X-ray exposure and a developer consisting of 40% methyl isobutyl ketone (MIBK) and 60% isopropyl alcohol (IPA). (In this and in all our work to date, we use PMMA with an average molecular weight of 950,000, and take certain steps³³ to remove any low molecular weight fragments prior to use.) A simple empirical expression for the linewidth of the final PMMA grating which is valid for a limited range of PMMA thicknesses can be obtained. To determine the exact profile which would be obtained for any particular shadowed triangular profile mask, a full simulation is necessary. Assuming a PMMA thickness of $\sim 2000 \text{ \AA}$, a tungsten thickness of $\sim 200 \text{ \AA}$, and a development latitude of a factor of 2, the linewidth, l , in angstroms for a grating period, d , in angstroms is given $\pm 50 \text{ \AA}$ by

$$l = d \frac{\tan \theta}{\tan \theta + \sqrt{2}} - 100 \text{ \AA} .$$

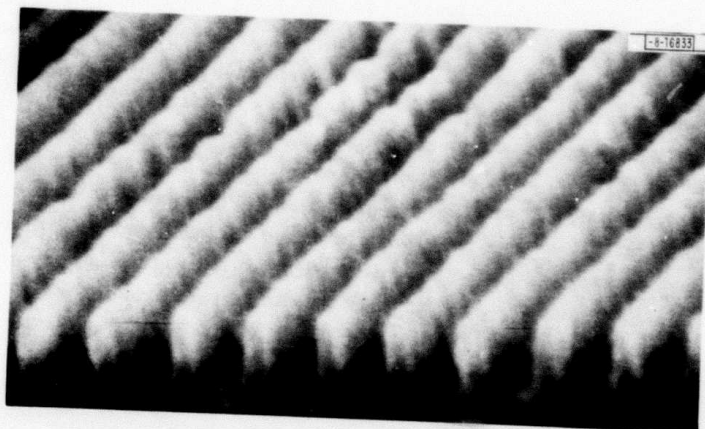
The linewidths that can be obtained directly by shadowing triangular cross-section masks range from near zero, obtained by shadowing at a very shallow angle, to a maximum determined by the total width of the angled sidewalls of the triangular polyimide structure. The opening can be no smaller than the flat portion of the relief structure. The largest linewidth is obtained by shadowing both sides of the structure. Larger linewidth to period ratios (i.e., smaller spaces) can be obtained by a two-step process. First, a narrow linewidth X-ray mask is made by shadowing a triangular profile polyimide mask. This mask is then replicated and the resulting PMMA structure used to produce a reversed contrast mask by liftoff or plating.

Figure 17 shows a scanning electron microscopy (SEM) micrograph of a $1\text{-}\mu\text{m}$ -period triangular profile relief structure in a $1\text{-}\mu\text{m}$ -thick polyimide membrane made by the process depicted in Figs. 14 and 15. One area of this structure was shadowed at 19° with 200 \AA of tungsten, another area was shadowed at 33° with 200 \AA of tungsten, and a third area was shadowed from both sides at 33° . The resulting mask was then replicated in PMMA using the carbon K X-ray. The mask and substrate were held in intimate contact during replication using an electrostatic hold-down scheme² in which a voltage is applied between the mask and substrate (usually a SiO_2 -coated silicon wafer). The mask was made conductive by evaporating a thin layer of aluminum on the smooth side of the polyimide membrane. The carbon K X-ray source was a conventional electron bombardment type operated at 4.7 kV at 400 W with a spot diameter of $\sim 1 \text{ mm}$ at a distance of 6 cm from the substrate. Exposure times were $\sim 150 \text{ min}$, giving a development rate of 33 \AA/sec in 40% MIBK and 60% IPA. The resulting 1500-, 3500-, and 7000- \AA linewidth structures are shown in Fig. 18. Figure 19(a) shows an SEM micrograph of a 3200- \AA -period grating having a 500- \AA linewidth which was exposed in 2000 \AA of PMMA using a triangular cross-section mask shadowed with 200 \AA of tungsten at 19.5° . Figure 19(b) shows an SEM micrograph of a 400- \AA -linewidth grating having a 1968- \AA period which was exposed using a mask shadowed with 200 \AA of tungsten at 25.2° . The linewidths obtained agree closely with the calculated values.



500 Å → | | ←
 ─────────────────────────────────── 3200 Å

(a)



400 Å → | | ← ─────────────────────────────────── 1 μm

(b)

Fig. 19. SEM micrograph of PMMA gratings on amorphous SiO_2 substrates produced by carbon K X-ray replication of shadowed triangular profile polyimide membrane X-ray masks. (a) Mask used had a 3200-Å period and was shadowed at 19.5° with 200 Å of tungsten; (b) mask used had a 1968-Å period and was shadowed at 25.2° .

For linewidths smaller than 400 \AA , it is more appropriate to fabricate the X-ray mask by shadowing a square-wave cross-section relief structure. This mask fabrication procedure is illustrated in Fig. 20. A square-wave surface-relief structure is first fabricated in SiO_2 by methods described in an earlier paper.²⁰ A polyimide replica of the structure is shadowed at an angle yielding the mask structure shown in Fig. 20. The relative X-ray attenuation of the wide and narrow regions can be such that by overexposure and/or overdevelopment only the narrow high-contrast region of the mask will be replicated in PMMA. A 3200-\AA -period square-wave structure was made in polyimide by the process shown in Fig. 20 and shadowed at an angle of 30° with 200 \AA of tungsten yielding a mask with a 180-\AA -wide linewidth and 8 dB of contrast. This mask was replicated in 600-\AA -thick PMMA using the carbon K X-ray source described above. To view the results of such a high resolution exposure, TEM is preferred over SEM because of the much higher resolution of the former. Figure 21 shows a TEM micrograph of a 600-\AA -high, 200-\AA -wide line which resulted from the exposure. To make the micrograph, a tungsten shadowed carbon replica was made of the relief structure exposed in the PMMA. Also shown is a perspective view of the structure as determined from the micrograph.

Because extremely smooth vertical sidewalls can be obtained in square-wave relief structures, masks with linewidths smaller than 100 \AA can be made. By shadowing such structures alternately with tungsten and an X-ray transparent material such as carbon, high-contrast X-ray masks with lines and spaces less than 100 \AA in width can be made. Such masks are ideally suited for investigating the ultimate resolution of X-ray lithography and for generating simple device geometries. Using a multiple shadowed square-wave mask, 175-\AA lines and spaces have been replicated in PMMA with the carbon K X-ray. Details of this research are given elsewhere.³⁴

A new technique for producing high-contrast X-ray masks with precisely controlled linewidths has been demonstrated. Soft X-ray replication of 200-\AA linewidths in PMMA on a thick SiO_2 substrate is reported. This is the smallest linewidth achieved by X-ray lithography up to the present and is the smallest linewidth structure produced by any lithographic technique on a thick substrate. Not only does this new mask fabrication technique provide a means of testing the ultimate resolution of X-ray lithography, it also opens the possibility of new classes of devices because of the small linewidths and unprecedented linewidth control which can be attained.

D. C. Flanders

Fig. 20. Sequence of steps for fabricating a shadowed square-wave profile polyimide X-ray mask. The SiO_2 square-wave structure is made by reactive-ion etching with CHF_3 through a chromium mask.

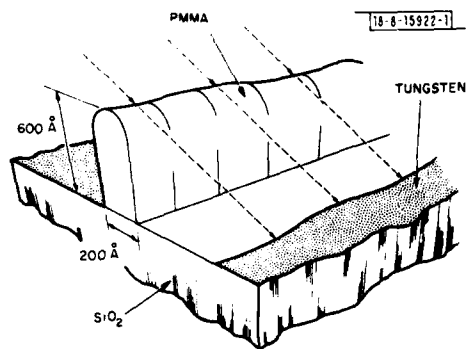
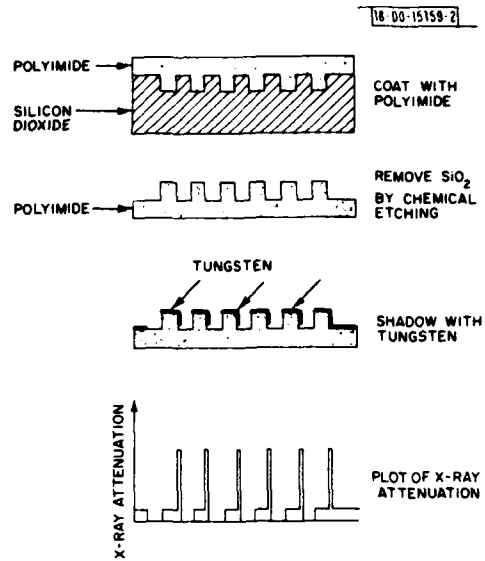


Fig. 21. TEM micrograph of a tungsten shadowed carbon replica of a 200-Å linewidth, 600-Å-high PMMA structure exposed with the carbon K X-ray on a thick SiO_2 substrate using a 3200-Å-period shadowed square-wave polyimide membrane X-ray mask. The perspective view of the original PMMA structure shown was deduced from the micrograph of the carbon replica.



REFERENCES

1. D. C. Flanders and H. I. Smith, *J. Vac. Sci. Technol.* 15, 1001 (1978).
2. D. C. Flanders, "Orientation of Crystalline Overlayers on Amorphous Substrates by Artificially Produced Surface Relief Structures," Ph. D. Thesis, Department of Electrical Engineering and Computer Science, Massachusetts Institute of Technology, February 1978; reprinted as Technical Report 533, Lincoln Laboratory, M.I.T. (5 December 1978), DDC AD-A071168.
3. H. I. Smith and D. C. Flanders, *Appl. Phys. Lett.* 32, 349 (1978).
4. D. C. Flanders, D. C. Shaver, and H. I. Smith, *Appl. Phys. Lett.* 32, 597 (1978); also D. C. Shaver, M. S. Thesis, Department of Electrical Engineering and Computer Science, Massachusetts Institute of Technology, September 1978.
5. H. I. Smith, D. C. Flanders, and D. C. Shaver, "New Applications of Submicrometer Structures in Materials Science and Biology," in *Scanning Electron Microscopy (1978)*, Vol. 1, pp. 33-40, O. Johari, Ed. (Scanning Electron Microscopy, Inc., 1978).
6. M. W. Geis, D. C. Flanders, and H. I. Smith, *Appl. Phys. Lett.* 35, 71 (1979).
7. D. C. Flanders, H. I. Smith, H. W. Lehmann, R. Widmer, and D. C. Shaver, *Appl. Phys. Lett.* 32, 112 (1978); H. W. Lehmann and R. Widmer, *Appl. Phys. Lett.* 32, 163 (1978); and erratum *Appl. Phys. Lett.* 33, 367 (1978).
8. K. E. Bean, *IEEE Trans. Electron Devices* ED-25, 1185 (1978).
9. P. D. DeGraff and D. C. Flanders, *J. Vac. Sci. Technol.* 16, 1906 (1979).
10. K. F. Lee, J. F. Gibbons, K. C. Saraswat, and T. I. Kamins, *Appl. Phys. Lett.* 35, 173 (1979).
11. J. F. Gibbons, K. F. Lee, T. J. Magee, J. Peng, and R. Ormond, *Appl. Phys. Lett.* 34, 831 (1979).
12. N. N. Sheftal, "Trends in Real Crystal Formation and Some Principles for Single Crystal Growth," in *Growth of Crystals (1976)*, Vol. 10, pp. 185-210, N. N. Sheftal, Ed. (Consultants Bureau, Plenum, New York, 1976).
13. A. Yariv, *Sci. Am.* 240, 64-72 (1979).
14. A. Yariv and M. Nakamura, *IEEE J. Quantum Electron.* QE-13, 232-253 (1977).
15. H. Sakaki, K. Wagatsuma, J. Hamasaki, and S. Saito, *Thin Solid Films* 36, 497 (1976).
16. H. I. Smith, S. R. Chinn, and P. D. DeGraff, *J. Vac. Sci. Technol.* 12, 1262-1265 (1975).
17. D. C. Shaver, D. C. Flanders, H. I. Smith, and N. M. Ceglio, *J. Vac. Sci. Technol.* 16, 1626 (1979).
18. D. C. Flanders, H. I. Smith, H. W. Lehmann, R. Widmer, and D. C. Shaver, *Appl. Phys. Lett.* 32, 112-114 (1978).
19. C. V. Shank and R. V. Schmidt, *Appl. Phys. Lett.* 23, 154-155 (1973).
20. G. C. Bjorklund, S. E. Harris, and J. F. Young, *Appl. Phys. Lett.* 25, 451-452 (1974).
21. T. Winthrop and C. R. Worthington, *J. Opt. Soc. Am.* 55, 373-381 (1965).
22. D. C. Flanders, *J. Vac. Sci. Technol.* 16, 1615 (1979).
23. R. A. McCorkle and H. J. Vollmer, *Rev. Sci. Instrum.* 48, 1055-1063, (1977).
24. K. Knop, *Opt. Commun.* 18, 298-303 (1976).

25. G. Schmahl and D. Rudolph, Progress in Optics, Vol. XIV (North Holland, Amsterdam, 1976).
26. H. Brauninger, P. Predehl, and K. P. Beuermann, Appl. Opt. 18, 368 (1979).
27. D. C. Flanders, D. C. Shaver, and H. I. Smith, Appl. Phys. Lett. 32, 597 (1978).
28. R. Feder, E. Spiller, and J. Topalian, J. Vac. Sci. Technol. 12, 1332 (1975).
29. R. Feder, E. Spiller, J. Topalian, and A. N. Broers, Science 197, 259 (1977).
30. J. L. Vossen and W. Kern, Thin Film Processes (Academic, New York, 1978), p. 465.
31. D. C. Flanders and H. I. Smith, J. Vac. Sci. Technol. 15, 995 (1978).
32. B. L. Henke and E. S. Ebisu, Advances in X-ray Analysis (Plenum, New York, 1974), Vol. 17, p. 150.
33. R. J. Hawryluk, "Energy Dissipation by Electron Beam Scattering in Thin Polymer Films," Ph. D. Thesis, Department of Electrical Engineering and Computer Science, Massachusetts Institute of Technology, 3 May 1974; and Technical Report 511, Lincoln Laboratory, M.I.T. (11 November 1974), DDC AD-A007061/5.
34. D. C. Flanders, Appl. Phys. Lett. 36, 93 (1980).

UNCLASSIFIED

SECURITY CLASSIFICATION OF THIS PAGE (When Data Entered)

REPORT DOCUMENTATION PAGE		READ INSTRUCTIONS BEFORE COMPLETING FORM
1. REPORT NUMBER 18 ESD-TR-79-311	2. GOVT ACCESSION NO. AD A088162	3. RECIPIENT'S CATALOG NUMBER
4. TITLE (and Subtitle) 6 Graphoepitaxy	5. TYPE OF REPORT & PERIOD COVERED 9 Semiannual Technical Summary rept. 1 January - 30 June 1979	6. PERFORMING ORG. REPORT NUMBER
7. AUTHOR(s) 10 Henry I. Smith	8. CONTRACT OR GRANT NUMBER(s) 15 F19628-78-C-0002 ✓ ARPA Order-3336	
9. PERFORMING ORGANIZATION NAME AND ADDRESS Lincoln Laboratory, M.I.T. P.O. Box 73 Lexington, MA 02173 16 0D10	10. PROGRAM ELEMENT, PROJECT, TASK AREA & WORK UNIT NUMBERS ARPA Order 3336 Program Element No. 61101E Project No. OD10	
11. CONTROLLING OFFICE NAME AND ADDRESS Defense Advanced Research Projects Agency 1400 Wilson Boulevard Arlington, VA 22209	12. REPORT DATE 11 30 June 1979	12. NUMBER OF PAGES 30
14. MONITORING AGENCY NAME & ADDRESS (if different from Controlling Office) Electronic Systems Division Hanscom AFB Bedford, MA 01731 12 29	15. SECURITY CLASS. (of this report) Unclassified	15a. DECLASSIFICATION DOWNGRADING SCHEDULE
16. DISTRIBUTION STATEMENT (of this Report) Approved for public release; distribution unlimited.		
17. DISTRIBUTION STATEMENT (of the abstract entered in Block 20, if different from Report)		
18. SUPPLEMENTARY NOTES None		
19. KEY WORDS (Continue on reverse side if necessary and identify by block number) surface-relief structures holographic lithography enhanced heteroepitaxy single-crystal films X-ray lithography thin film growth reactive-ion etching graphoepitaxy		
20. ABSTRACT (Continue on reverse side if necessary and identify by block number) Graphoepitaxy of silicon films, 0.5 μm thick, has been achieved on amorphous fused silica substrates by laser crystallization of amorphous silicon deposited over surface-relief gratings etched into the substrates by reactive-ion etching. A simple model for the graphoepitaxy process is presented. Sheet resistivity of phosphorus-doped graphoepitaxial silicon was 2.5 times larger than that of bulk silicon of the same doping. A technique is described for exposing patterns of spatial period p/n using near-field diffraction from masks of spatial period p. The technique, called "spatial-period-division," was used to double a 196.8-nm-period grating-pattern X-ray mask to produce a 98.4-nm-period pattern in PMMA. Exposure of higher spatial-frequency-multiples appears feasible. A new technique for fabricating high-contrast X-ray masks with precisely controlled linewidths is described. The technique is based on the deposition at an oblique angle ("shadowing") of X-ray absorber material onto relief structures of triangular or square cross section in a polyimide plastic membrane. Linewidth control of ±50 Å should be possible for submicrometer period gratings. The successful replication of <200-Å linewidth patterns in PMMA using the carbon K X-ray and shadowed square cross-section masks is reported.		

DD FORM 1473 EDITION OF 1 NOV 65 IS OBSOLETE
1 JAN 73UNCLASSIFIED
SECURITY CLASSIFICATION OF THIS PAGE (When Data Entered)

207650

Jlu